High-efficiency green and red phosphors enable a broader hue-gamut light-emitting diode backlight for brighter displays

Dieu An Nguyen Thi[1], Phan Xuan Le[2]
[1]Faculty of Electrical Engineering Technology, Industrial University of Ho Chi Minh City, Ho Chi Minh City, Vietnam
[2]Faculty of Mechanical-Electrical and Computer Engineering, School of Engineering and Technology, Van Lang University, Ho Chi Minh City, Vietnam

Article Info

ABSTRACT

In this article, we suggest combining a blue InGaN chip with strait-band green (β-sialon:Eu^{2+}) and red (K$_2$SiF$_6$:Mn^{4+}) phosphors to create white light-emitting diodes (WLED) devices with a wide hue range and high effectiveness that may be utilized in LCD backlighting. The highest radiation wavelength of a gas-pressure sinted β-sialon:Eu^{2+} is 535 nm, the full width at half maximum (FWHM) is 54 nm, and the outside quantum performance is 54.0% lower than the 450 nm stimulation. We created K$_2$SiF$_6$:Mn^{4+} in two steps. The phosphor possesses a sharp line radiation spectrum accompanied by the most intense maximum point under 631 nm, an FWHM reaching roughly 3 nm, as well as an exterior quantum effectiveness of 54.5%. When computed at 120 mA, the manufactured three-range wLEDs had an illuminating performance of 91–96 lm/W and a large color temperature of 11,184–13,769 K (i.e., 7,828–8,611 K in LCD screens). The hue range represented by the CIE 1931 and CIE 1976 hue gaps is 85.5-85.9% and 94.3-96.2% of the NTSC requirement, respectively. The optic characteristics outperform those of phosphor-transformed wLED backlights utilizing broad-range green or red phosphors, indicating the two strait-range phosphors studied are the best luminous substances for producing brighter and livelier screens.

Corresponding Author:

Phan Xuan Le
Faculty of Mechanical-Electrical and Computer Engineering, School of Engineering and Technology
Van Lang University
Ho Chi Minh City, Vietnam
Email: le.px@vlu.edu.vn

1. INTRODUCTION

Technologies are always changing, which makes it possible or enhance the picture quality and hue saturation of LCDs utilized in TVs, cellphones, computers, tablet PCs, and car navigators, with backlight technology playing a significant role in these advancements. Phosphor-transformed white light-emitting diodes (WLED) devices as well as quantum dot (QD) backlightings have lately emerged as potential replacements for traditional cold cathode-fluorescence lights (CCFL) backlights since these devices will become a slimmer, easier-to-carry, as well as more alive screen with greater light level [1]-[3]. When compare to CCFLs, which have a hue range reaching roughly 75% based on the national television standard committee (NTSC) requirement, three-range WLED devices could achieve a hue range exceeding 90% NTSC *Commission internationale de l'eclairage* (CIE) 1976, while QD backlightings expect a hue scale exceeding 100% NTSC. Even though QD backlightings possess the largest hue scope, they have various disadvantages, including size, expense, toxic effects, and longevity [4]-[6]. As a substitute to QDs made of

Cd, the safe InP/ZnS QDs produce a hue scale reaching 87% NTSC, which is significantly lower than the poisonous counterparts [7]. Phosphor-transformed WLED backlightings, on the contrary, which create a merger between a light-emitting diode (LED) chip emitting blue light and singular or many phosphors, would be widely utilized owing to the huge scale, low expense, strength, and high performance. Phosphors are one of the main parts in this technology that have a significant impact on the hue saturation and luminosity of LCDs.

In its beginning phases, WLED backlighting was created by mixing a wide-range YAG:Ce^{3+} phosphor emit yellow light with a blue-color LED. Nevertheless, the hue gamut of this form of the backlight is only 72% of the NTSC benchmark, making it difficult to give clear red and abundant image quality [8]. The tiny hue range achieved with YAG:Ce^{3+} is primarily owing to the excessive overlay among the green as well as red radiation spectra once the radiation spectrum bypasses RGB hue sievers utilized by LCDs to balance picture quality and energy usage. A dichromatic phosphor combination made of a green phosphor as well as a red phosphor provides an alternative solution. For instance, we developed a three-range WLED backlighting with a hue range of up to 92% NTSC [1] using promising green β-sialon:Eu^{2+} and red CaAlSiN$_3$:Eu^{2+} [9]-[11]. Xu *et al.* [12] assessed a fascinating green Sr$_3$Si$_{13}$Al$_3$O$_2$N$_{21}$:Eu^{2+} and succeeded in constructing a WLED backlighting with a 94.2% color scale [13], [14]. Anh *et al.* [15] obtained a 90% NTSC hue range by using green SrGa$_2$S$_4$:Eu^{2+} and red CaS:Eu^{2+} films for WLED backlighting. These findings imply that the brightness spectrum in green as well as red phosphors has a strong influence on the backlighting's hue range. Generally, phosphors for backlighting must emit in a strait-range and have a specific radiation maximum.

From a substance layout aspect, it is possible to make narrow-range phosphors; i) using accommodative triggers, like Eu^{2+}, within a symmetrical layout; and ii) using triggers with spin- or parity-prohibited electron transport, like Mn^{2+} and Mn^{4+}. The initial condition would be illustrated by β-sialon:Eu^{2+}, in which Eu^{2+} becomes harmozined with six O/N atoms under equal spacing, as well as the second by Sr[LiAl$_3$]N$_4$:Eu^{2+}, in which Eu^{2+} is bound to eight N atoms, which generates a polyhedron in cuboid form [16]. The FWHM for Eu^{2+} within certain hosts is substantially less than that of Eu^{2+} within the majority of hosts (55 nm compared to roughly 90 nm) due to the remarkable symmetry of the formation. Both Mn^{2+} and Mn^{4+} have remarkably tiny bandwidths, with the FWHM in Mn^{4+}-doped K$_2$SiF$_6$ usually being numerous nanometers owing to the spin-as well as parity-prohibited $^2E_g \rightarrow ^4A_{2g}$ transformation, meaning that γ-alon:Mn^{2+} and K$_2$SiF$_6$:Mn^{4+} can be promising strait-range green as well as red phosphors used in backlighting [17]. Besides bandwidth, different essential facets like quantum effectiveness, radiation maximum location, deteriorate period, and steadiness against heating and/or chemical damages must be taken into consideration when choosing phosphors for usage in wLED backlightings. In this regard, moisture-sensitive Sr[LiAl$_3$]N$_4$:Eu^{2+}, Sr$_2$GaS$_4$:Eu^{2+}, and CaS:Eu^{2+} are rarely utilized only if their stability is greatly improved.

Owing to their elevated performance, stability, and reliability, both the strait-range β-sialon:Eu^{2+} and the deep-red CaAlSiN$_3$:Eu^{2+} are widely regarded as the most effective phosphors for wLED backlightings. CaAlSiN$_3$:Eu^{2+}, on the other side, has some limitations that stop it from attaining a much greater hue gamut and greater backlight illumination: i) a wider radiation spectrum that covers a significant quantity of the spectral power loss after filtration, and ii) a huge spectral overlay among the stimulation band of colors of CaAlSiN$_3$:Eu^{2+} and the emitting spectrum of β-sialon:Eu^{2+}, which boosts the quantity of green-color phosphor used Figure 1. As a result, it is critical to look for a different strait-range red phosphor for the purpose of improving the hue regeneration as well as luminosity in the WLED backlighting. K$_2$SiF$_6$:Mn^{4+} is a strait-range red phosphor with five distinct line bands of colors at 609, 613, 631, 634, and 648 nm [18]. Until now, almost all research on K$_2$SiF$_6$:Mn^{4+} and its derivates has been focused on synthesis and implementation for WLED devices possessing great hue generation indicators in illumination. Jia *et al.* [19] prepared a WLED device with a hue heat reaching 3510K, Ra reaching 91, as well as illuminated effectiveness reaching 82 lm/W using KSF:Mn^{4+} and YAG:Ce^{3+}. Huang *et al.* [20] used KSF:Mn^{4+} to create a WLED with extremely high hue generation and parameters as follows: CRI of 94, R9 of 93, CCT of 2,700K, and 107 lm/W. These findings support the use of strait-range red phosphors to improve the hue rendition and luminescent effectiveness of white LEDs. From our understanding, KSF:Mn^{4+} has only been mentioned and illustrated for application in WLED backlightings on a few occasions. Swiatczak *et al.* [21] prepared WLEDs for application in liquid crystal display (LCD) backlightings using K$_2$SiF$_6$:Mn^{4+} in the form of a red phosphor as well as Sr$_2$GaS$_4$:Eu^{2+} as a green phosphor [22]. Even then, owing to its humidity sensitivity, Sr$_2$GaS$_4$:Eu^{2+} is rarely utilized in practical screens. In this study, we tried to create a merger between strait-range KSF:Mn^{4+}, β-sialon:Eu^{2+} and an InGaN blue LED, resulting in a brighter (95 lm/W) as well as wider hue range exceeding 96% NTSC) WLED backlighting when comparing to earlier researches.

2. EXPERIMENTAL METHODS

2.1. Creating green-emitting β-sialon:Eu²⁺ phosphor

A gas pressure sintering approach was used to create β-sialon:Eu^{2+}(Si$_{6-z}$Al$_z$O$_z$N$_{8-z}$:Eu^{2+}, z=0.5, 0.5 at % Eu). A suitable quantity of α-Si$_3$N$_4$, AlN, Al$_2$O$_3$, as well as Eu$_2$O$_3$ were measured and thoroughly combined by hand in a mortar. We put a sum of 2 g of the powder combination inside a boron nitride crucible, then set on fire within a gas-pressure sintering furnace accompanied by a graphite firing device. The specimen was warmed up in a vacuum (<10^{-3} Pa) at a steady rate of 600 °C/h from normal temperature to 800 °C. Under this temperature, we added a nitrogen gas (99.999%) to the room. The temperature reached 2,050 °C. We then fired the substance for 12 hours at the heat underneath a nitrogen gas pressure measured at 1.0 MPa. We disabled the power after the firing step, and the substance were left to cool in a furnace. For ohter usages, we pulverized, cleaned, then strained the heated phosphor powder.
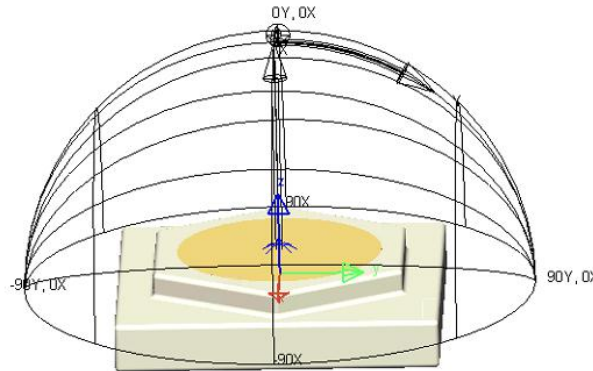

Figure 1. Photograph of WLEDs

2.2. Characterization of phosphor

At room temperature, radiancy spectra were calculated with a fluorescent spectrophotometer and a 200 W Xe light as a stimulation origin. An illuminating diffuser and a tungsten lamp were used to rectify the radiation spectrum to rouse the spectral reaction for a monochrometer as well as a photomultiplier pipe (Noma, 10 V, 4 A). With rhodamine-B in the form of a reference, the stimulation spectrum was rectified for the spectral dispersion of xenon light strength as well.

Timing-resolved PL assessments were mentioned with a timing-correlated single-photon counting fluorometer outfitted with a Nano LED (λ_{em}=370 nm) and a pulse length of time full breadth at half-maximum of ~1ns. We measured the radiancy correlated with temperature in the multichannel photodetector accompanied by a Xe light working under 200 W in the form of a stimulation source to assess heat quenching. We put the phosphor powder in a hot plate connected with the MPCD-7000, then fired it to the required temperatures at a 100 °C-per-minute speed. We kept the substance under a specific heat for 5 minutes for the task of achieving heat balance. This ensures homogeneous temperature allocation on the exterior as well as interior of the substance. A QE-1100 phosphor quantum productivity spectrophotometer was used to measure temperature-dependent quantum effectiveness. The equations below [23]-[25] were used to measure external (η_0), internal (η_i) quantum efficiencies (QEs), and absorbing efficacy (α_{abs}):

$$\eta_0 = \frac{\int \lambda \bullet P(\lambda)d\lambda}{\int \lambda \bullet E(\lambda)d\lambda} \tag{1}$$

$$\eta_i = \frac{\int \lambda \bullet P(\lambda)d\lambda}{\int \lambda \{E(\lambda)-R(\lambda)\}d\lambda} \tag{2}$$

$$\alpha_{abs} = \frac{\int \lambda \{E(\lambda)-R(\lambda)\}d\lambda}{\int \lambda \bullet E(\lambda)d\lambda} \tag{3}$$

$E(\lambda)/h\nu$, $R(\lambda)/h\nu$, and $P(\lambda)/h\nu$ indicate the amount of photons for the phosphor's stimulation, reflectance, and radiation spectrums, respectively. The phosphor film of actual MCW-LEDs is reproduced using flat silicone films and the LightTools 9.0 application and the Monte Carlo technique. This method is applied over two different stages: (1) Establishing, building the layout as well as optical characteristics of MCW-LED lamps (2). The β-sialon:Eu^{2+} concentration variation then controls the optical impacts of the phosphor combining. To assess the influence of YAG:Ce^{3+} as well as β-sialon:Eu^{2+} combining on the output

in MCW-LED lights, we need to draw several similitudes. It is specified that the two kinds of dual-film distant phosphor, having CCT levels reaching 3,000 K; 4,000 K; and 5,000 K need to be defined. Figure 1 illustrates a thorough description for MCW-LED lamps having conformal phosphor combining along with 8,500-K CCT. The layout of multi-chip white LED lamps (MCW-LEDs) with parts other than β-sialon:Eu^{2+} is also considered. The reflector's bottom lengthiness reaches 8 mm, pitch reaches 2.07 mm, and highest exterior lengthiness reaches 9.85 mm. The protective-coating phosphor combination surrounds nine chips that are 0.08-mm thick. All chips are connected with the reflector cavity via a 1.14-mm^2 square base as well as a 0.15-mm height. The luminous flux for each chip reaches 1.16 W, having a maximum wavelength of 453 nm.

3. RESULTS AND ANALYSIS

Figure 2 depicts the inverse shift in the concentration of green phosphorus β-sialon:Eu^{2+} and yellow phosphorus YAG:Ce^{3+}. This alteration has two purposes: retaining median CCT values, and affecting the absorptivity as well as dispersion within the WLED device with two phosphor films, see Figure 2(a). This essentially influences the hue quality and illuminating flux effectiveness of WLEDs. Thus, the β-sialon:Eu^{2+} concentration chosen determines the hue quality of WLEDs. When the β-sialon:Eu^{2+} concentration raised (2%-20%) by weight, the YAG:Ce^{3+} concentration lowered for the task of retaining the mean CCTs. It is also true for WLEDs with hue temperatures ranging between 5,600 K and 8,500 K, as displayed in Figure 2(b).

Figure 3 shows the impact of β-sialon:Eu^{2+} green phosphorus concentration on the transmission spectrum in the WLED device. We have to pick an option by judging the required demands. WLED devices with good hue fidelity can diminish luminance by a tiny amount. As seen in Figure 3(a), white illumination appears to be made from the spectral area. The spectrum of 5,000 K is depicted in this graphic. Plainly, the intensity trend rises with β-sialon:Eu^{2+} content in two sections of the light spectrum: 420-480 nm as well as 500-640 nm. Such a shift of the two-range radiation spectra indicates superior luminance. Furthermore, the dispersion of blue illumination in WLED is improved, implying that diffusing in the phosphorous film and in WLEDs is risen, favoring hue uniformity. Such an outcome would be remarkable if we utilize β-sialon:Eu^{2+}. Managing the hue homogeneity for the distant phosphor configuration huge temperature, particularly, proves to be challenging, proving that β-sialon:Eu^{2+}, under small as well as great hue heats (5,600 K as well as 8,500 K) may enhance the hue standard in the WLED device, see Figure 3(b). Thus, the article demonstrated the efficacy of the emitted light flux of this dual-sheet distant phosphor layer, see Figure 4. The results of Figures 4(a) and (b) indicate that the luminance rises dramatically when the concentration of β-sialon:Eu^{2+} rises (2%-20% wt.). The hue divergence was severely diminished tandem to the phosphor β-sialon:Eu^{2+} concentration under every CCT level, which is the results in Figure 5. Such an event is the result of the red phosphor film's absorptivity. When the β-sialon:Eu^{2+} phosphor absorbs blue lighting generated by the LED chip, the blue phosphor granules turn the illumination to green illumination, see Figure 5(a). The β-sialon:Eu^{2+} particles absorb the light of yellow additionally to the blue illumination generated by the chip. However, owing to the absorption features of the substance, the blue light absorbing from the LED chip is stronger when compared to these two absorbs. Due to introducing β-sialon:Eu^{2+}, the green illumination concentration within the WLED device grows, leading to superior hue homogeneity, as shown Figure 5(b). Hue uniformity would be one crucial feature among present WLED factors. Consequently, the higher the hue uniformity, the greater the cost of WLED. By employing β-sialon:Eu^{2+}, we would benefit from its inexpensive expense. β-sialon:Eu^{2+} can thus be broadly utilized.
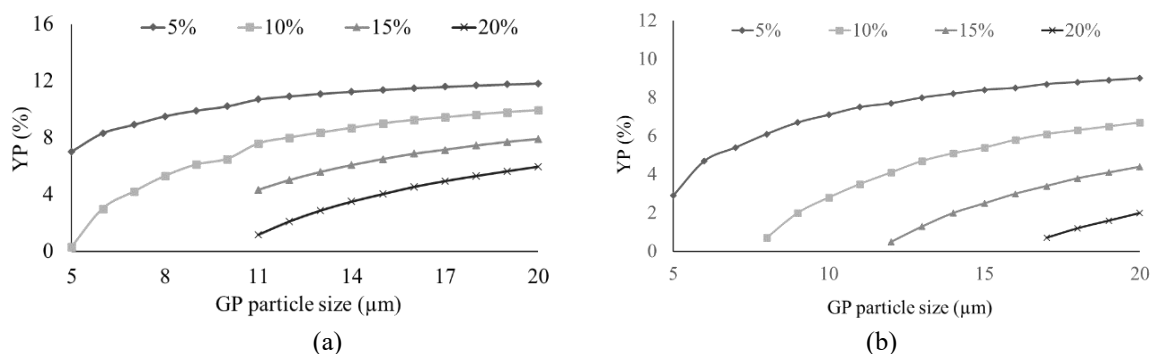

Figure 2. Adjusting phosphor concentration for the task of retaining CCTs: (a) 5,000 K and (b) 6,500K
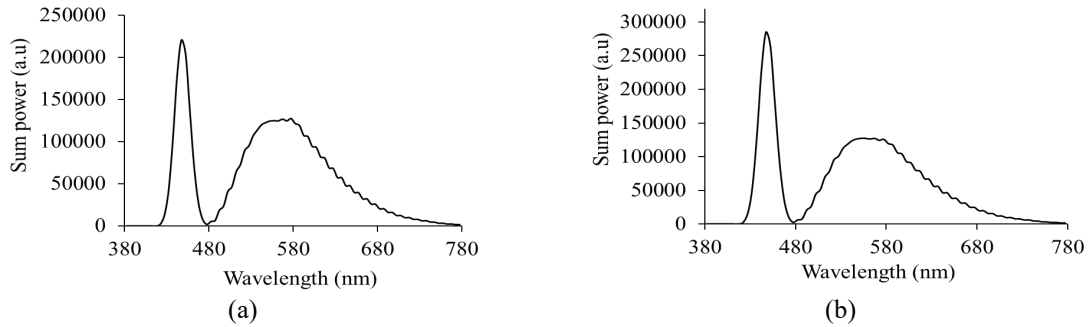
Figure 3. The radiation spectra in 5000 K WLED device along with β-sialon:Eu^{2+} concentration:
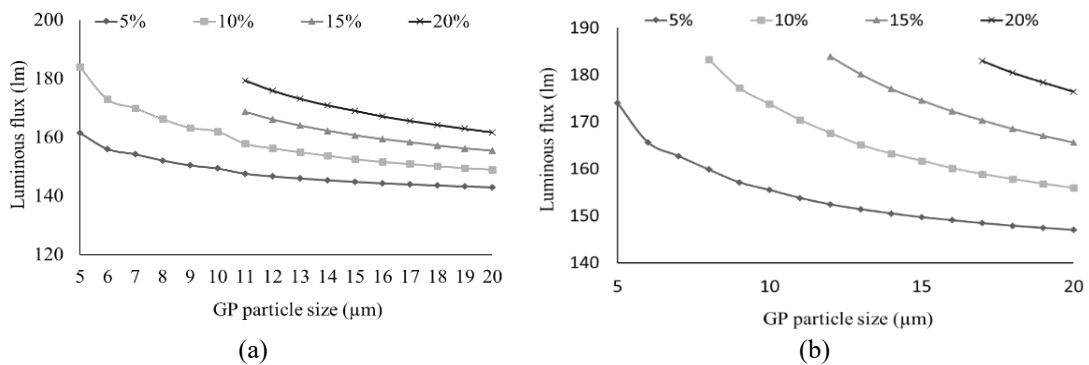(a) 5,000 K and (b) 6,500K

Figure 4. The lighting beam in WLED device along with β-sialon:Eu^{2+} concentration: (a) 5,000 K and
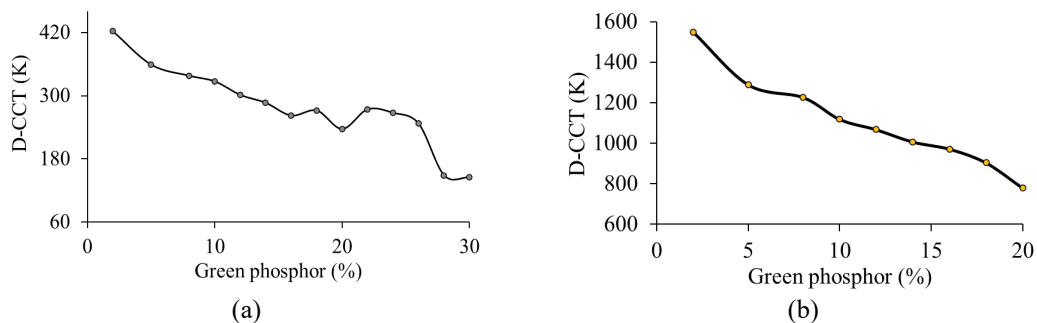(b) 6,500 K

Figure 5. The hue deviation in WLED device along with β-sialon:Eu^{2+} concentration: (a) 5,000 K and
(b) 6,500 K

Hue uniformity is only one element to pay attention to when evaluating the hue quality of WLEDs. Hue quality can not be claimed to be excellent with a great hue homogeneity indicator. As a result, subsequent studies give a hue rendering indicator and a hue quality scale. When an illumination shines on the hue rendering index, it determines the genuine hue for an object. The hue imbalance is generated by green illumination's overwhelming presence among the primary hues: green, blue, as well as yellow, which has an impact on the hue quality of WLEDs, resulting in a reduction in WLED hue accuracy. The results in Figure 6 show a small decline in CRI in the presence of the distant phosphor β-sialon:Eu^{2+} layer. However, these are acceptable because CRI is simply a drawback of CQS, see Figure 6(a). When contrasting CRI to CQS, the latter would be of greater necessity as well as tougher to obtain, as shown in Figure 6(b). It contains three facets: the hue generation indicator, beholder's desire, as well as hue coordinate. With the factors, CQS can be nearly a genuine overall assessment for hue quality. Figure 7 demonstrates the CQS rise when the sheet of remote phosphor β-sialon:Eu^{2+} is added. Furthermore, when the β-sialon:Eu^{2+} concentration grows, CQS undergoes little changes with β-sialon:Eu^{2+} concentrations below 10% wt, see Figure 7(a). If the β-

sialon:Eu^{2+} concentration goes beyond 10% wt., CRI, along with CQS is dramatically lowered, a result of severe waste of hue if green becomes dominant as displayed in Figure 7(b). Consequently, when utilizing green phosphor β-sialon:Eu^{2+} proper concentration choice is critical.
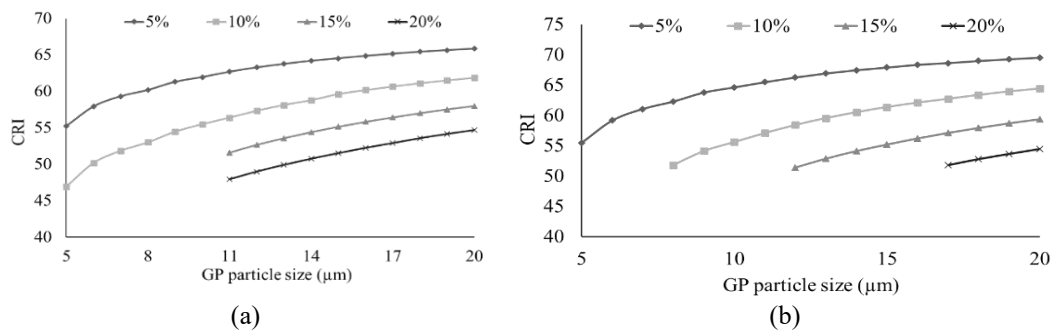

Figure 6. The hue rendering indicator in WLED device along with β-sialon:Eu^{2+} concentration:
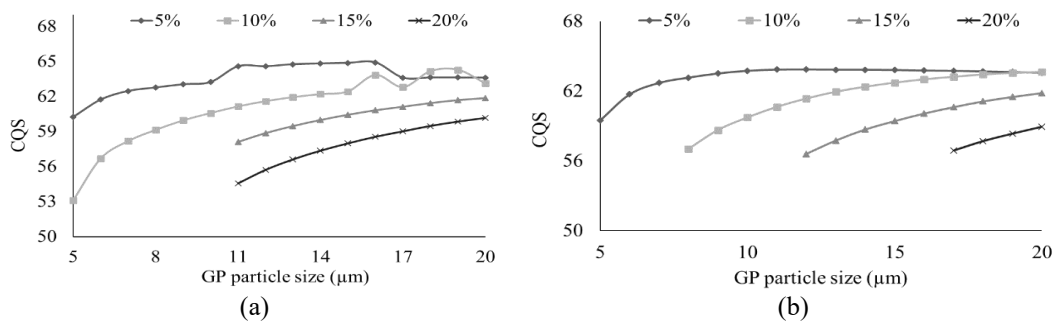(a) 5,000 K and (b) 6,500 K

Figure 7. The CQS in WLED device along with β-sialon:Eu^{2+} concentration: (a) 5,000 K and
(b) 6,500 K

4. CONCLUSION

The article shows the effect of β-sialon:Eu^{2+} green phosphorus on the optical properties of a dual-sheet phosphor structure. β-sialon:Eu^{2+} would be a promising option when it comes to augmenting hue consistency under Monte Carlo technique, which applies to WLEDs with a low hue temperature of 5,000 K, as well as those having a hue temperature exceeding 8,500 K. The outcomes of this investigation have therefore achieved the goal of improving hue quality and illuminating flux, which is particularly hard due to the distant structure of phosphorus. Nonetheless, there is one small limitation hindering CRI as well as CQS. If the β-sialon:Eu^{2+} concentration rises considerably, the CRI and CQS fall dramatically. As a result, according to the manufacturer's goals, the appropriate concentration must be chosen. The article has provided a wide range of new material for reference in generating higher hue uniformity and lighting flux WLEDs.

REFERENCES

[1]   M. Giliberto, F. Arena, and G. Pau, "A fuzzy-based solution for optimized management of energy consumption in e-bikes," *Journal of Wireless Mobile Networks, Ubiquitous Computing, and Dependable Applications*, vol. 10, no. 3, pp. 45–64, 2019, doi: 10.22667/JOWUA.2019.09.30.045.

[2]   H. Aljarajreh, D. D. C. Lu, Y. P. Siwakoti, R. P. Aguilera, and C. K. Tse, "A method of seamless transitions between different operating modes for three-port DC-DC converters," *IEEE Access*, vol. 9, pp. 59184–59195, 2021, doi: 10.1109/ACCESS.2021.3073948.

[3]   Y. C. Liu, J. Zhang, C. K. Tse, C. Zhu, and S. C. Wong, "General pathways to higher order compensation circuits for IPT converters via sensitivity analysis," *IEEE Transactions on Power Electronics*, vol. 36, no. 9, pp. 9897–9906, Sep. 2021, doi: 10.1109/TPEL.2021.3062228.

[4]   F. Arena and G. Pau, "An overview of big data analysis," *Bulletin of Electrical Engineering and Informatics*, vol. 9, no. 4, pp. 1646–1653, Aug. 2020, doi: 10.11591/eei.v9i4.2359.

[5]   S. Feng *et al.*, "Color lensless in-line holographic microscope with sunlight illumination for weakly-scattered amplitude objects," *OSA Continuum*, vol. 2, pp.9-16, 2019, doi: 10.1364/OSAC.2.000009.
[6]   A. J. Henning *et al.*, "Improvements to dispersed reference interferometry: beyond the linear approximation," *Appl. Opt*, vol. 58, pp. 131-136, 2019, doi: 10.1364/AO.58.000131.
[7]   R. Deeb *et al.*, "Deep spectral reflectance and illuminant estimation from self-interreflections," *J. Opt. Soc. Am. A,* vol. 36, pp. 105-114, 2019, doi: 10.1364/JOSAA.36.000105.
[8]   S. Kumar *et al.*, "Extended light-source-based lensless microscopy using constrained and regularized reconstruction," *Appl. Opt,* vol. 58, pp. 509-516, 2019, doi: 10.1364/AO.58.000509.
[9]   F. Jiang *et al.*, "Efficient InGaN-based yellow-light-emitting diodes," *Photon. Res*, vol. 7, 144-148, 2019, doi: 10.1364/PRJ.7.000144.
[10]   A. I. Alhassan *et al.*, "Development of high performance green c-plane III-nitride light-emitting diodes," *Opt. Express*, vol 26, pp. 5591-5601, 2018, doi: 10.1364/OE.26.005591.
[11]   S. Jost *et al*, "CIE 2017 color fidelity index Rf: a better index to predict perceived color difference?," *J. Opt. Soc. Am. A*, vol 35, pp. B202-B213, 2018, doi: 10.1364/JOSAA.35.00B202.
[12]   Q. Xu *et al.*, "Testing uniform colour spaces using colour differences of a wide colour gamut," *Opt. Express*, vol. 29, pp. 7778-7793, 2021, doi: 10.1364/OE.413985.
[13]   M. Quesada *et al.*, "All-glass, lenticular lens light guide plate by mask and etch," *Opt. Mater. Express*, vol. 9, pp. 1180-1190, 2019, doi: 10.1364/OME.9.001180.
[14]   P. Kumar *et al.*, "Enhanced exclusive-OR and quick response code-based image encryption through incoherent illumination," *Appl. Opt*, vol. 58, pp. 1408-1412, 2019, doi: 10.1364/AO.58.001408.
[15]   N. D. Q. Anh *et al.*, "Selection of a remote phosphor configuration to enhance the color quality of white LEDs," *Curr. Opt. Photon*, vol. 3, pp. 78-85, 2019, doi: 10.3807/COPP.2019.3.1.078.
[16]   Y. Li *et al.*, "395 nm GaN-based near-ultraviolet light-emitting diodes on Si substrates with a high wall-plug efficiency of 52.0%@350 mA," *Opt. Express*, vol. 27, pp. 7447-7457, 2019, doi: 10.1364/OE.27.007447.
[17]   J. Hao *et al.*, "Prediction of lifetime by lumen degradation and color shift for LED lamps, in a non-accelerated reliability test over 20,000 h," *Appl. Opt*, vol. 58, pp. 1855-1861, 2019, doi: 10.1364/AO.58.001855.
[18]   Y. Yang *et al.*, "Low complexity OFDM VLC system enabled by spatial summing modulation," *Opt. Express*, vol. 27, pp. 30788-30795, 2019, doi: 10.1364/OE.27.030788.
[19]   J. Jia *et al.*, "Three-wavelength passive demodulation technique for the interrogation of EFPI sensors with arbitrary cavity length," *Opt. Express*, vol. 27, pp. 8890-8899, 2019, doi: 10.1364/OE.27.008890.
[20]   C. Huang *et al.*, "Bandwidth correction of spectral measurement based on Levenberg–Marquardt algorithm with improved Tikhonov regularization," *Appl. Opt*, vol. 58, pp. 2166-2173, 2019, doi: 10.1364/AO.58.002166.
[21]   B. Swiatczak *et al.*, "Changes in fundus reflectivity during myopia development in chickens," *Biomed. Opt. Express*, vol. 10, pp. 1822-1840, 2019, doi: 10.1364/BOE.10.001822.
[22]   H. Feuk, D. Sanned, M. Richter, and M. Aldén, "Sources of error for single-shot PMT-based phosphor thermometry in harsh conditions, " *Measurement Science and Technology*, vol. 32, no. 8, p. 084003, Aug. 2021, doi: 10.1088/1361-6501/abfb1e.
[23]   L. I. D. J. Martin, D. Poelman, P. F. Smet, and J. J. Joos, "Microscopic Study of dopant distribution in europium doped $SrGa_2S_4$: Impact on thermal quenching and phosphor performance," *ECS Journal of Solid State Science and Technology*, vol. 7, no. 1, pp. R3052–R3056, Sep. 2018, doi: 10.1149/2.0341709jss.
[24]   X. Zhu *et al.*, "Synthesis and Characterization of Er^{3+}-Doped $SrNb_2O_6$ Phosphor for FIR Based Thermometer," *ECS Journal of Solid State Science and Technology*, vol. 10, no. 4, p. 046001, Apr. 2021, doi: 10.1149/2162-8777/abf0ea.
[25]   E. Hertle *et al.*, "(Gd,Lu)AlO3:Dy3+ and (Gd,Lu)3Al5O12:Dy3+ as high-temperature thermographic phosphors," *Measurement Science and Technology*, vol. 30, no. 3, p. 034001, Mar. 2019, doi: 10.1088/1361-6501/aafcac.

BIOGRAPHIES OF AUTHORS

Dieu An Nguyen Thi [iD] [g] [SC] [P] received a master of Electrical Engineering, HCMC University of Technology and Education, VietNam. Currently, she is a lecturer at the Faculty of Electrical Engineering Technology, Industrial University of Ho Chi Minh City, Vietnam. Her research interests are Theoretical Physics and Mathematical Physics. She can be contacted at email: nguyenthidieuan@iuh.edu.vn.

Phan Xuan Le [iD] [g] [SC] [P] received a Ph.D. in Mechanical and Electrical Engineering from Kunming University of Science and Technology, Kunming city, Yunnan province, China. Currently, He is a lecturer at the Faculty of Engineering, Van Lang University, Ho Chi Minh City, Vietnam. His research interests are Optoelectronics (LED), Power transmission and Automation equipment. He can be contacted at email: le.px@vlu.edu.vn.